



HAL
open science

Air-blown gasification of Solid Recovered Fuels (SRFs) in lab-scale bubbling fluidized-bed: Influence of the operating conditions and of the SRF composition

Maxime Hervy, Damien Remy, Anthony Dufour, Guillain Mauviel

► To cite this version:

Maxime Hervy, Damien Remy, Anthony Dufour, Guillain Mauviel. Air-blown gasification of Solid Recovered Fuels (SRFs) in lab-scale bubbling fluidized-bed: Influence of the operating conditions and of the SRF composition. *Energy Conversion and Management*, 2019, 181, pp.584-592. 10.1016/j.enconman.2018.12.052 . hal-01969508

HAL Id: hal-01969508

<https://hal.univ-lorraine.fr/hal-01969508>

Submitted on 4 Jan 2019

HAL is a multi-disciplinary open access archive for the deposit and dissemination of scientific research documents, whether they are published or not. The documents may come from teaching and research institutions in France or abroad, or from public or private research centers.

L'archive ouverte pluridisciplinaire **HAL**, est destinée au dépôt et à la diffusion de documents scientifiques de niveau recherche, publiés ou non, émanant des établissements d'enseignement et de recherche français ou étrangers, des laboratoires publics ou privés.

1 **Air-blown gasification of Solid Recovered Fuels (SRFs) in lab-scale bubbling fluidized-bed:**
2 **influence of the operating conditions and of the SRF composition**

3 Maxime Hervy, Damien Remy, Anthony Dufour, Guillaïn Mauviel*

4 LRGP, CNRS, Université de Lorraine, ENSIC, 1, Rue Grandville, Nancy, France

5 Corresponding author at: guillaïn.mauviel@univ-lorraine.fr

6 **Abstract**

7 This article investigates the gasification of Solid Recovered Fuels (SRFs). To better understand the
8 influence of SRF composition on gasification efficiency and syngas quality, two industrial SRFs having
9 different compositions were studied. A detailed SRF characterization was performed (elemental
10 analysis; ash composition; LHV; fraction of biomass, non-biomass, and inert materials) to precisely
11 describe the chemical complexity of such materials. The gasification tests were performed at pilot-scale
12 in a bubbling fluidized bed using air as gasifying agent, and olivine as bed material. The separate
13 contribution of gasification temperature ($T=750-900^{\circ}\text{C}$) and equivalence ratio ($ER=0.21-0.35$) on the
14 gasification efficiency was investigated by sequentially varying these two parameters.

15 Gasification tests revealed that the LHV of the syngas and the cold gas efficiency decreased by 45-50%
16 and by 20-30%, respectively, with rising equivalence ratio. These evolutions were attributed to syngas
17 oxidation reactions which promoted the formation of CO_2 . Indeed, mass balances calculation revealed
18 that the part of carbon atoms in syngas in the form of CO_2 rises from 43 to 54% for SRF1, and from 35
19 to 50% for SRF2. High plastic content in SRF2 was responsible for the formation of stable light
20 hydrocarbons (CH_4 , C_2H_4 and C_6H_6) from the decomposition of the plastic polymer chains, and to lower
21 amount of H_2 compared to syngas from biomass-rich SRF1. The carbon conversion decreased by 8%
22 with rising ER from 0.21 to 0.30 for SRF2, as a result of plastics-biomass interactions promoting
23 secondary reactions and leading to char formation. For both SRFs, rising temperature significantly
24 improved the gasification efficiency whatever the SRF composition, and decreased the CO_2
25 concentration. These evolutions were attributed to the promotion of several reactions, such as
26 gasification, steam and dry reforming, Boudouard reaction, and Reverse Water-Gas Shift reaction.

27 **1. Introduction**

28 Nowadays, the worldwide MSW generation is around 1.3 billion tons per year, and is expected to reach
29 2.2 billion tons per year by 2025 [1]. Despite the recent progresses in waste management, the collection,
30 recycling and valorization of waste still have to be strongly improved. Indeed, around 47 % of the
31 wastes generated in EU are disposed in landfill sites [2], leading to air and soil pollution. In order to
32 manage the increasing worldwide generation of municipal solid wastes, new solutions must be

33 developed. Thermal treatment plants, such as incineration, are essential for the management of
34 municipal wastes [3,4]. In a comprehensive review, *Arena* summarized the main advantages of thermal
35 treatments, including: (a) the reduction of waste mass and volume leading to significant saving of land
36 compared to landfilling, (b) the destruction of contaminants, or (c) the concentration of inorganic
37 species in the ashes [5]. Incineration is the most known and optimized thermal process as it is operated
38 at industrial scale for many years. However, gasification process appears as a promising way for waste
39 valorization due to the numerous applications existing for the gasification gas, named syngas. While
40 flue gas from combustion can be valorized solely by transferring its thermal energy to heat carriers
41 (typically steam), the syngas can be used as a fuel in high efficiency processes such as gas engine, gas
42 turbine, fuel cell, or as a precursor for liquid fuel synthesis (*via* the Fischer-Tropsch reaction) and
43 chemicals production (methanol). Another advantage of gasification is that the syngas can be valorized
44 under different forms in other times and places, while the heat produced by combustion must be
45 consumed directly.

46 Solid recovered fuels (SRFs) consist of a mixture of non-hazardous solid wastes, such as plastics,
47 textiles, tires, paper and carton, biomass waste, or sludge. SRFs are very complex and heterogeneous
48 materials, and the fraction of each component can vary significantly depending on the waste origin, the
49 season, the waste separation plant, and the SRF production technique. SRFs represent a significant
50 waste resource, estimated at 90 million tons per year in France. The production of energy from the non-
51 recyclable fraction of the SRF thus appears as an attractive solution for waste management. The high
52 diversity of SRFs chemical composition does not allow to precisely define the nature of this fuel, which
53 makes difficult the development of valorization processes. In an attempt of clarification, a classification
54 was established by a French professional organization of recycling companies (FEDEREC). SRFs are
55 classified into four classes depending on the standards defined for the following parameters: lower
56 heating value; density; particle size; halogen compounds concentration; sulfur, nitrogen and ash
57 contents. A better definition of SRF is expected to facilitate the development of specific valorization
58 routes having better energy efficiency than the actual use of SRF as fuel in cement kiln.

59 Gasification consists of a partial oxidation of the solid fuel at high temperature (800-1000 °C) using an
60 oxidizing agent (air, steam, O₂ or CO₂). The solid fuel is mainly decomposed into syngas, a mixture of
61 partially oxidized species (H₂, CO, CO₂, CH₄, C_nH_m) having high calorific value. Gasification process
62 has been intensively investigated for biomass valorization, but the presence of pollutants in the syngas
63 (such as tar, acid gases, and particulate matter) compromises its valorization [6].

64 Different gasification technologies have been developed. Among them, fluidized bed reactor appears
65 as the most suitable for medium-size processes (1 to 100 MW), due to the efficient flow mixing between
66 reactants, the carefully controlled temperature, the high heat transfer performance, and the large
67 operating flexibility allowing to use different kinds of fuels, including biomass and solid wastes [7–9].

68 Air-blown bubbling fluidized bed was proved to efficiently convert different wastes in syngas: meat
69 waste and wastewater treatment sludge [10,11], tires [12,13], poultry fuel [14], plastic wastes [15,16],
70 municipal solid waste [17,18], biomass waste [19,20], and solid recovered fuels [21,22]. Olivine,
71 dolomite, and sand are the most frequently used bed materials in fluidized bed reactor. Sand can be used
72 as bed material to ensure the fluidization, but has insignificant catalytic activity in tar cracking reaction.
73 To improve the gasification efficiency and the syngas quality, catalysts can be used as bed materials.
74 Dolomite is the low-cost catalyst having the highest catalytic activity in tar reforming reactions [22].
75 Dolomite can also prevent bed agglomeration when the fuel gasified is rich in alkaline and alkaline
76 earth metals [23]. The main drawback of dolomite consists in its attrition tendency which significantly
77 increases the dust pollution in syngas from fluidized bed. On the contrary, olivine presents strong
78 mechanical properties despite relatively low catalytic activity in tar cracking reactions [22,24]. Olivine
79 is often used as bed material in fluidized bed reactors, which reduces the dust load in syngas, and
80 slightly decreases the tar content. Other types of materials have been tested, and their pros and cons are
81 reported in the comprehensive review of *Shen et al.* [25].

82 At industrial scale, the gasifiers are autothermal, but it is not the case at lab-scale because the walls of
83 small reactors must be heated to balance the heat loss. As a consequence, temperature and ER are
84 independent conditions, whereas temperature depends on ER at industrial scale. In the past few years,
85 SRFs gasification was increasingly studied in lab-scale fluidized beds, and the effect of the operating
86 conditions on gasification behavior was investigated. Increasing equivalence ratio (ER) was proved to
87 promote the oxidation reactions which increases both the syngas yield and the carbon conversion
88 [26,27]. Similar results were obtained with the gasification of other wastes [10,28]. Oxidation reactions
89 decreased the content of H₂, CO, CH₄ and light hydrocarbon compounds [29–31], resulting in a drop of
90 the syngas LHV and of the CGE. The influence of the temperature has also been investigated. Rising
91 gasification temperature at a fixed ER value increases the syngas yield and carbon conversion [28].
92 Globally, the cold gas efficiency (CGE) decreased with increasing temperatures due to the drop in
93 syngas LHV [26,27]. Contradictory results were reported about the evolution of the CH₄ content and of
94 the LHV of the syngas. While *Berrueco et al.* found that they reached a maximum at 800 °C before to
95 decrease with higher temperature [26,27], *Dunnu et al.* reported that they increased with rising
96 temperature from 800 to 850 °C [21]. These opposite trends can result from the different SRF
97 composition, but a lack of study devoted to the influence of the SRF composition prevents to conclude
98 this point.

99 Most of the already published articles mainly focused on “synthetic” SRF consisting in the mixture of
100 well-known plastics and biomass, without taking into consideration the complexity of a real SRF
101 composition. In the present paper, two industrial SRFs having different chemical compositions have
102 been used to improve the understanding of the SRFs composition influence on the gasification
103 efficiency. A detailed characterization of SRFs was performed. Gasification temperature and

104 equivalence ratio (ER) have been sequentially varied in order to identify their separate contribution on
105 the gasification efficiency. The syngas composition was measured on-line with a μ -GC allowing to
106 analyze permanent gases and BTX. Gasification efficiency was analyzed based on four indicators: cold
107 gas efficiency (CGE), carbon conversion (CC), syngas lower heating value (LHV_{syngas}), and the syngas
108 yield (η_{syngas}). The distribution of hydrogen and carbon atoms in the gaseous products was determined
109 and discussed based on SRF composition and gasification conditions.

110 **2. Materials and methods**

111 **2.1 Characterization of the Solid Recovered Fuels**

112 The two SRFs samples were provided by different French companies. The elemental composition was
113 measured according to the standard NF EN 15407. The ash content was measured at 550°C according
114 to the standard NF EN 15403. The composition of the resulting ashes was measured by X-Ray
115 Fluorescence Spectroscopy. This technique was chosen to cope with the problem of the silica
116 mineralization required for ICP analysis. The Br, Cl, and F contents were specifically determined by
117 ionic chromatography according to the standards NF EN 15408 and NF EN ISO 10304-1. The Lower
118 Heating Value (LHV) of the SRF was measured with a calorimetric bomb (NF EN 15400). The
119 proportion and composition of biomass, non-biomass, and inert materials were determined according
120 to the French standard NF EN 15 440.

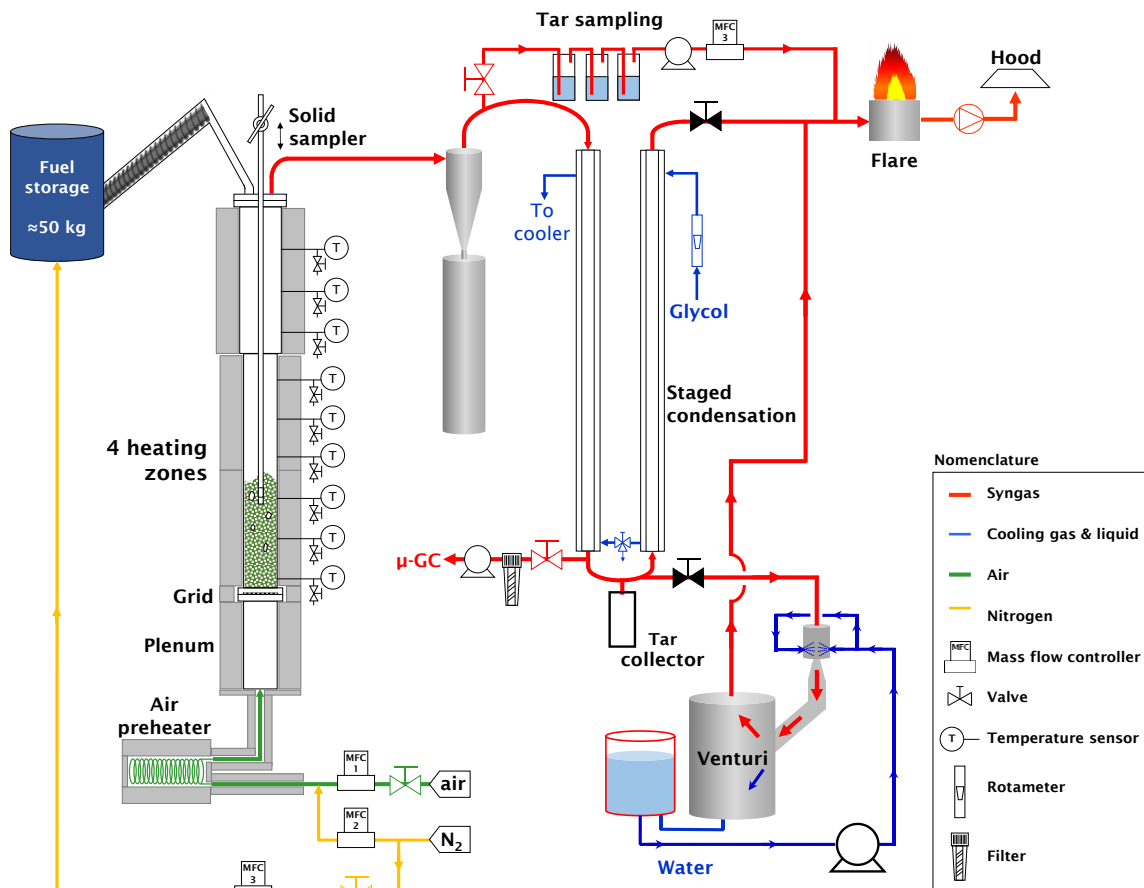
121 **2.2 Gasification reactor**

122 Gasification tests were performed in a bubbling fluidized-bed constructed in our laboratory and
123 presented in a previous article [32]. The gasifier is divided into three zones: the plenum (d=100 mm,
124 H=300 mm), the bed zone (d=100 mm, H=800 mm), and the freeboard zone (d=140 mm, H=800 mm)
125 (Figure 1). The gasifying agent was air whose flowrate was controlled by a mass flow controller (Brooks
126 5850S). At the bottom of the gasifier, a 3mm thick inox grid was used as distributor plate to homogenize
127 the air flow and insure an efficient fluidization. The gasifier is heated by eight electrical heater shells at
128 a maximum temperature of 1000 °C.

129 SRFs were fed at the top of the reactor with a sloping screw. Around 3 kg of olivine was placed in the
130 gasifier. The particle size distribution of this olivine is presented in Figure S.1 (in Supplementary
131 Material). At 800°C, the minimum fluidization velocity (U_{mf}) was measured at 0.15 m/s at 800 °C in
132 the reactor by progressively increasing the air flowrate while measuring the pressure drop in the gasifier.
133 At the gasifier outlet, the syngas flowed through a cyclone to remove particles, before to be cooled with
134 two air heat exchangers. A water Venturi scrubber was also used to remove tar and acid gases before
135 flaring the syngas. The gasifier is equipped with 19 lateral tubes allowing to locally measure the bed
136 and freeboard temperatures. Pressure was continuously measured below the grid and at the top of the
137 freeboard zone. The syngas was sampled before the Venturi scrubber (see Figure 1) and analyzed on-

138 line by a μ -GC (Varian micro-GC 490) every 3 minutes. Permanent gases N_2 , CO , CO_2 , H_2 , CH_4 , C_2H_2 ,
 139 C_2H_4 , C_2H_6 , C_3H_4 , C_3H_6 , and C_6H_6 were quantified with this technique.

140 At the end of the experiment, the bed material (olivine+ash+char) was recovered after being cooled
 141 under a pure N_2 sweep gas. Its velocity was lower than the minimum fluidization velocity to avoid the
 142 mixing of the bed. A solid sampler was introduced through the top of the gasifier and its vertical position
 143 was set. This system allowed sampling 100 mm thick bed layers.

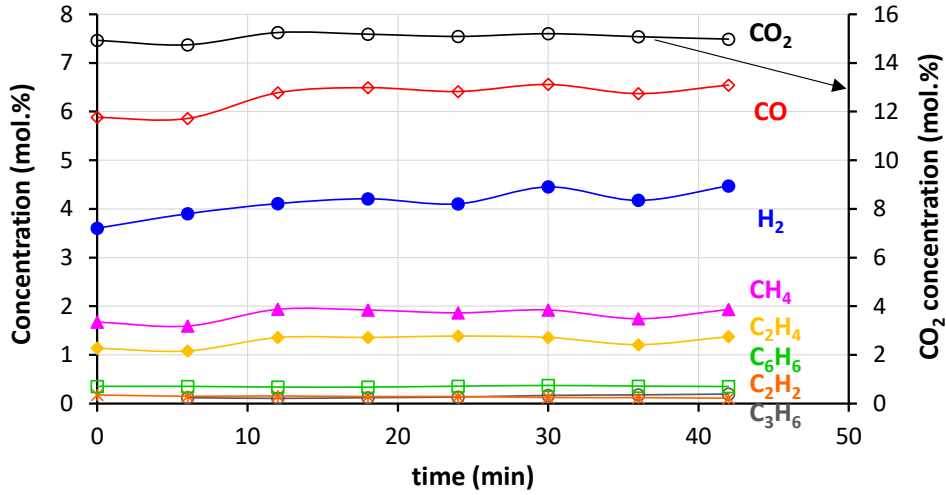


144

145 *Figure 1: Scheme of the gasification device.*

146 **2.3 Gasification conditions**

147 Before starting the gasification tests, the system was preheated at the desired temperature (750-900 °C)
 148 under air. When the temperature was close to the gasification temperature, the air flowrate was set at
 149 the desired value. The air velocity was 4 times the minimum fluidization velocity, corresponding to an
 150 air flowrate of 4.5 m³/h (STP). Once the temperatures were stable along the gasifier, the gasification
 151 started by feeding the SRF at a controlled flowrate, corresponding to the desired ER. When the
 152 gasification conditions were stable (gasifier temperature, and syngas composition analyzed by μ -GC),
 153 the permanent regime was maintained at least 40 minutes before to be modified (Figure 2).



154

155 *Figure 2: Example of permanent regime reached during the gasification of SRF1 at 800 °C with*
 156 *ER=0.30.*

157 During the tests, either the temperature or the equivalence ratio (ER) was changed. ER is defined as the
 158 operating air flowrate divided by the air flowrate required for the stoichiometric SRF oxidation. In this
 159 study, the ER was varied between 0.21 and 0.35. The SRF tank was continuously flushed with 10
 160 NL/min of pure N₂ to avoid the degradation of the fuel in the feeding screw. This flowrate was taken
 161 into consideration for the results analysis by using N₂ as a tracer for the calculation of the syngas
 162 flowrate.

163 2.4 Evaluation of the gasification performance

164 The gasification efficiency is mainly evaluated based on four indicators calculated from experimental
 165 results. As benzene is not a problematic compound for syngas valorization in gas engine [33], it is taken
 166 into account in these calculations. The lower heating value of the dry syngas (LHV_{syngas}) is calculated
 167 from a weighted average of the molar LHV of each gas (including benzene) and is expressed in MJ/m³
 168 (STP) of syngas (including N₂), according to Eq.1:

$$169 \quad \text{LHV}_{\text{syngas}} = \frac{\sum_i \left(\frac{\text{LHV}_i}{x_i} \right)}{V_m} \quad \text{Eq.1}$$

170 Where V_m represents the molar volume of ideal gas at STP (22.4 L/mol), and x_i the molar fraction of
 171 the gas species i.

172 The syngas yield (η_{syngas}) corresponds to the volume of dry syngas produced (including N₂) by kg of
 173 SRF (on dry ash free basis), and was calculated according to Eq.2:

$$174 \quad \eta_{\text{syngas}} = \frac{Q_{\text{Vsyngas}}}{Q_{\text{mSRF}}} \quad \text{Eq.2}$$

175 Where Q_{Vsyngas} is the volumetric syngas flowrate including N₂ (m³/h STP) which is calculated using N₂
 176 as a tracer, and Q_{mSRF} the mass flowrate of SRF (kg_{daf}/h).

177 The carbon conversion (CC) expresses the percentage of carbon transferred from SRF to syngas, and is
 178 calculated by Eq.3:

$$179 \quad CC = Q_{m_{syngas}} * M_C * \frac{\sum_i \left(\frac{X_i}{M_i} * n_i^C \right)}{Q_{m_{SRF}} * X_C^{SRF}} * 100 \quad \text{Eq.3}$$

180 Where $Q_{m_{syngas}}$ is the mass flowrate of syngas (kg/h), M_C is the molecular weight of carbon, n_i^C is the
 181 number of carbon atoms in the molecule i, X_C^{SRF} is the mass fraction of carbon in SRF (on daf basis),
 182 and X_i and M_i are respectively the mass fraction of the gas i in the syngas and its molecular weight.

183 Finally, the last indicator is the Cold Gas Efficiency (CGE), expressed in %, reflecting the fraction of
 184 chemical energy transferred from SRF to syngas:

$$185 \quad CGE = \frac{\eta_{syngas} * LHV_{syngas}}{LHV_{SRF}} * 100 \quad \text{Eq.4}$$

186 **3. Results**

187 **3.1 Physico-chemical properties of the SRF**

188 The two SRF studied were provided by two French companies and produced from distinct waste
 189 separation facilities managing different pristine types of wastes. Therefore, they represent interesting
 190 and complementary materials having different compositions (Table 1). SRF1 is ash-rich (>35 wt.%)
 191 and relatively poor in carbon (≈ 36 wt.%). On the contrary, the SRF2 is rich in carbon (52.6 wt.%) and
 192 contains relatively small amount of ash (18.5 wt.%). The oxygen content is almost similar for the two
 193 SRF (≈ 20 wt.%). SRF2 has a significantly higher LHV than SRF1 (Table 1), resulting from the lower
 194 ash content of SRF2.

195 The ash composition of the SRF was analyzed after combustion by XRF (Table 1). The ashes of SRF2
 196 have high Ca and Si contents (35 and 30 wt.%, respectively). It can be noted that SRF1 and SRF2
 197 present a significant concentration of Al (18.53 and 17.44 wt.%). SRF1 contains the highest amount of
 198 Si (40.51 wt.%). Its CaO content is significant (25.86 wt.%) but remains lower than that of SRF2. The
 199 results also showed that the two SRF are Br-free, but contain both Cl and F (Table 1). According to the
 200 French classification, SRF2 is in class 4 due to its significant Cl content, while SRF1 is in class 2.

201 *Table 1: Elemental analysis, ash composition, and lower heating value of the SRF.*

	SRF1	SRF2
Elemental analysis (dry wt.%)		
C	36.3	52.6
H	4.9	7.2
N	1.4	1.3
S	0.3	0.2
O	20.0	20.3
Ash	37.1	18.5

Ash composition (wt.%)		
SiO ₂	40.51	29.75
Al ₂ O ₃	17.44	18.53
Fe ₂ O ₃	4.94	5.52
TiO ₂	1.14	2.19
CaO	25.86	34.65
MgO	4.78	2.42
Na ₂ O	1.28	3.82
K ₂ O	1.15	0.76
SO ₃	0.44	0.70
P ₂ O ₅	2.24	1.43
MnO ₂	0.16	0.10
SrO	0.06	0.11
Total	100.0	100.0
Br, Cl, and F contents (wt.%)		
Br	<i>nd</i>	<i>nd</i>
Cl	0.39	1.16
F	0.02	0.01
LHV (MJ/kg_{dry})		
	14.3	22.4

nd: lower than 0.002 wt.%

202

203 **Table 2** presents the proportion and composition of biomass, non-biomass, and inert materials
 204 composing the two SRFs. SRF1 contains the higher fractions of inert and biomass materials (10.6 and
 205 55.2 wt.%, respectively). Its biomass fraction mainly consists in fines and paper/cartons, while glass
 206 roughly composes the inert fraction. This latter explains its significant SiO₂ content measured by XRF.
 207 The SRF2 mainly consists in non-biomass materials (**Table 2**) predominantly composed of plastics.
 208 Indeed, plastics represent 65 wt.% of SRF2. SRF2 was inert-free, and its biomass fraction was
 209 composed of textiles, paper/cartons, and wood. These characterizations demonstrate that the two
 210 selected SRFs have significantly different compositions.

211 *Table 2: Proportion and composition of biomass, non-biomass, and inert materials in the SRF.*

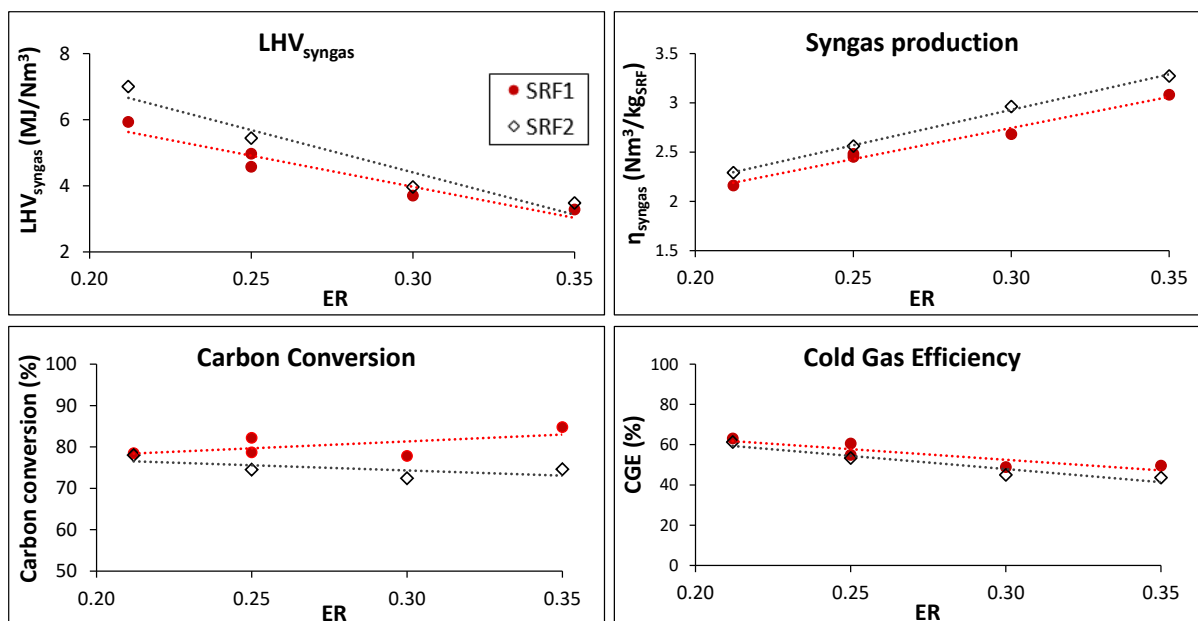
	SRF1	SRF2
Biomass fraction (wt.% dry)	55.2	27.8
paper/carton	44.9	29.3
wood	1.3	16.3
textiles	0.0	30.0
fines<10mm	53.8	24.4
Non-biomass fraction (wt.% dry)	34.3	72.4
plastics	13.3	90.7
carpet/matress	0.0	0.0
fines<10mm	86.4	9.3
Inert fraction (wt.% dry)	10.6	0.0
ferrous metals	0.0	0.0
non-ferrous metals	0.0	0.0
rocks	13.8	0.0
glass	86.2	0.0

212 3.2 Gasification of the SRF

213 3.2.1 Influence of the Equivalence Ratio

214 To study the separate influence of the Equivalence Ratio (ER) on the gasification efficiency,
215 the SRFs were gasified at a temperature of 810-825 °C controlled by the electrical heater shells. The
216 ER was adjusted from 0.21 to 0.35 by modifying the SRF flowrate (between 2.3 and 5.9 kg/h on dry
217 basis) while keeping a constant air flowrate in order to maintain similar fluidization conditions.

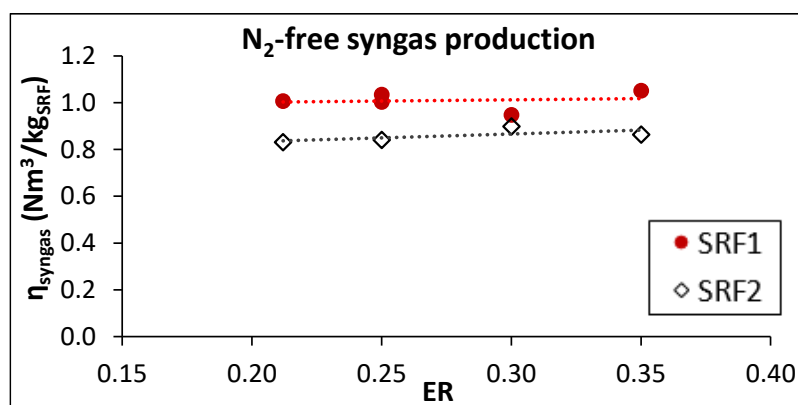
218 The evolutions of the cold gas efficiency (CGE), carbon conversion (CC), syngas yield (η_{syngas}),
219 and lower heating value of the syngas ($\text{LHV}_{\text{syngas}}$) versus ER are presented in Figure 3. Whatever the
220 SRF composition, it can be observed that increasing ER led to: (i) a slight decrease of the CGE; (ii) a
221 significant increase in syngas yield; and (iii) a decrease of the $\text{LHV}_{\text{syngas}}$. These results are in agreement
222 with previous studies [18,30]. However, the carbon conversion evolution depended on the SRF
223 composition. In the range $0.21 < \text{ER} < 0.35$, the CC increased by 6.8% for SRF1, while it decreased by
224 5.6% for SRF2. This difference can be attributed to the large amount of ash in SRF1 (35 wt.%),
225 especially to the inorganic species known for their catalytic activity in gasification reaction (such as Ca,
226 Na, K or Fe) [34], which could catalyze the carbonaceous matter conversion. In addition, the type of
227 plastics presents in SRF significantly influence the carbon conversion. For example, interactions
228 occurring during the co-gasification of black polycarbonate and polyethylene-terephthalate with
229 biomass were found to increase the carbon conversion, while no interaction was observed with
230 polypropylene [35]. Moreover, other interactions could occur between plastics and biomass to enhance
231 the char yield by promoting secondary reactions (condensation, polymerization), which decrease the
232 carbon conversion [36]. A precise analysis of the plastic fractions would be required to elucidate the
233 evolution of carbon conversion. Part of the carbon initially contained in the SRF was present in tars and
234 fly ash generated during the gasification test, which explains that the carbon conversion is lower than
235 100%.



236

237 *Figure 3: Evolution of the syngas Lower Heating Value (LHV_{syngas}), the syngas production (η_{syngas}), the*
 238 *carbon conversion (CC) and the Cold Gas Efficiency (CGE) with the ER at a temperature of 800-*
 239 *820°C.*

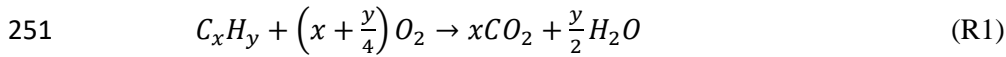
240 The increase in syngas yield with rising ER is explained by the higher ratio of air to SRF in the gasifier.
 241 If one subtracts the nitrogen from the outlet gas flowrate, the syngas yield (*i.e.* the gas produced) slightly
 242 increased with rising ER (Figure 4). However, it can be observed that the syngas production was around
 243 20% higher with SRF1.



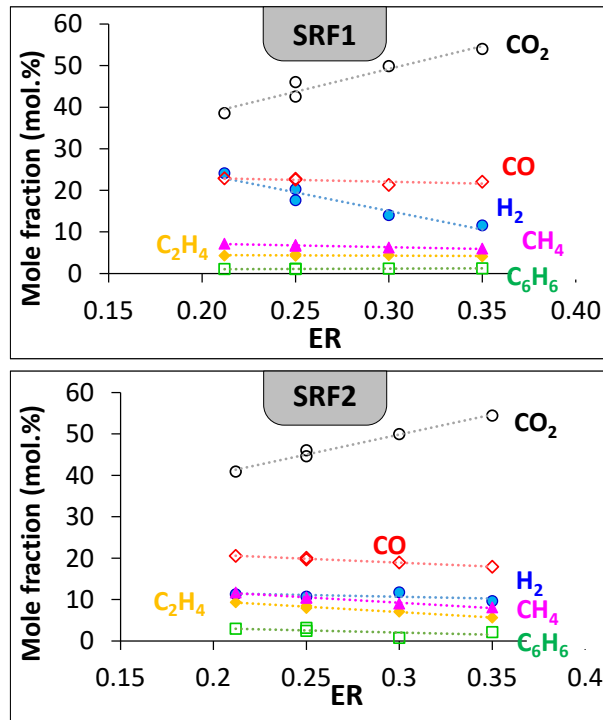
244

245 *Figure 4: Evolution of the syngas yield free of nitrogen with ER.*

246 To better understand the relationships between the SRF composition and the gasification phenomenon,
 247 the syngas composition was also studied. Table S.1 (in Supplementary Material) presents the syngas
 248 composition at the gasifier outlet, while Figure 5 displays the composition of the gas produced by
 249 gasification (nitrogen free). Rising ER decreased the fraction of the produced gases, except for CO₂.
 250 This latter increased due to the syngas oxidation reactions promoted by increasing ER (R1):

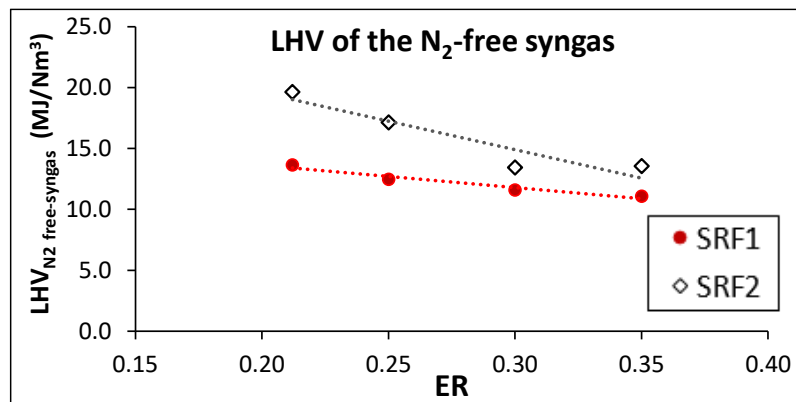


252 This reaction also contributed to the decrease of the LHV_{syngas} with increasing ER. Indeed, the LHV of
 253 the N₂-free syngas was proved to decrease with increasing ER (Figure 6). Plastic-rich SRF2 presented
 254 higher LHV_{syngas} than biomass-rich SRF1, which is in agreement with a previous study [15].



255
 256 *Figure 5: Evolution of the composition of the gas produced (without nitrogen) with ER for the*
 257 *different SRFs at a temperature of 800-820°C.*

258 For SRF2, H₂ and CH₄ display similar evolution and comparable concentration with rising ER (Figure
 259 5). However, for SRF1, the H₂ content was significantly higher than that of CH₄, especially at low ER.
 260 The H₂/CH₄ ratio was equal to 3.4 at ER=0.21, and to 1.9 at ER=0.35.



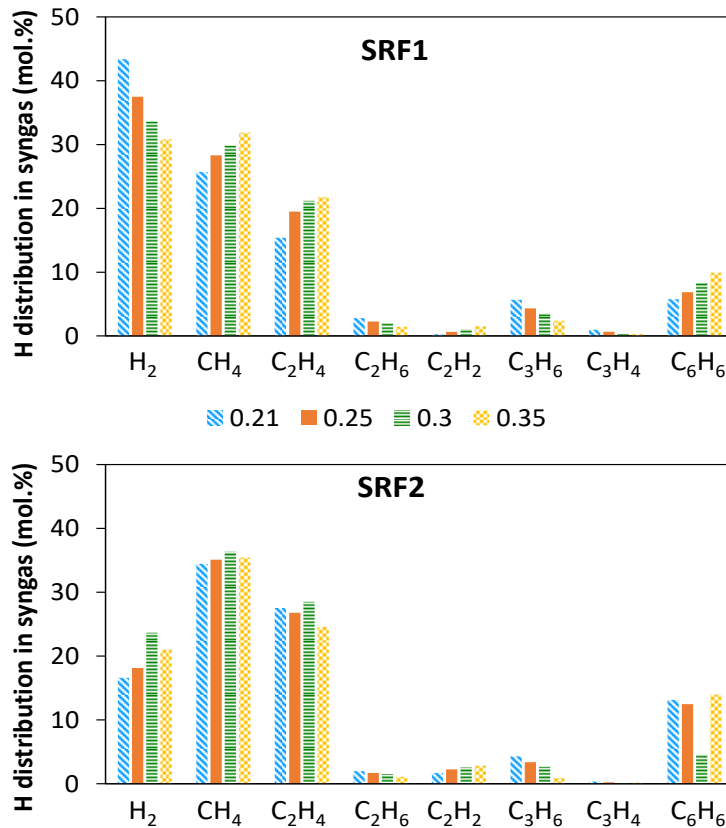
261
 262 *Figure 6: Evolution of the Lower Heating Value of the N₂-free syngas with (ER).*

263

264 To go further in the H-species composition, the distribution of H atoms in the gaseous products was
 265 calculated, according to Eq.(5):

$$266 \quad S_H^i = \frac{n_H^i * F^i}{\sum_k (n_H^k * F^k)} \quad \text{Eq.5}$$

267 Where S_H^i is the molar selectivity representing the fraction of H atoms present in the syngas in the form
 268 of the molecule i , n_H^k is the number of H atom in the molecule k , and F^k is the molar flowrate of the gas
 269 k .



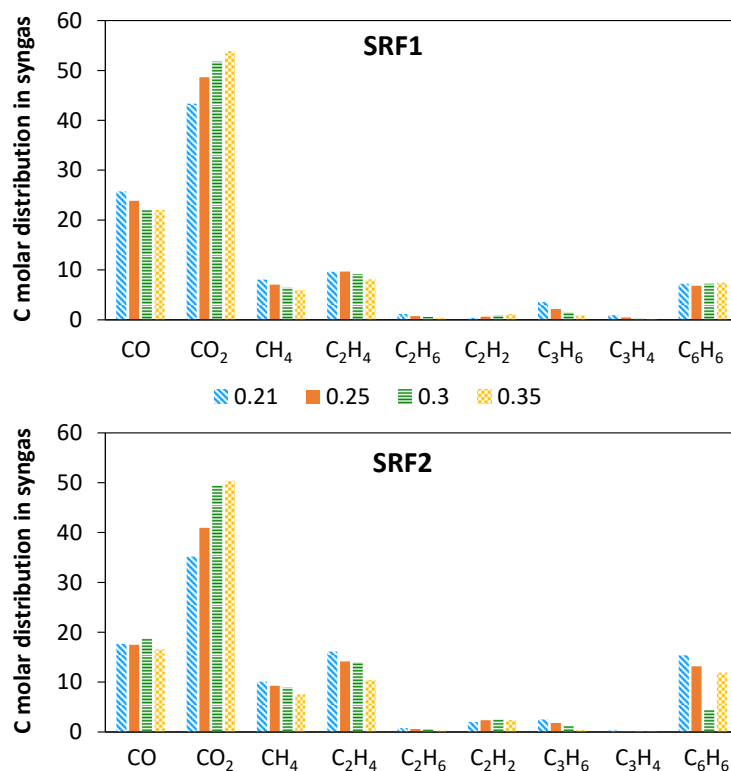
270

271 *Figure 7: Molar distribution of hydrogen in H-containing gases depending on the ER at a*
 272 *temperature of 800-820 °C.*

273 The results, presented in Figure 7, confirm that H₂ was the main H-containing gas produced during the
 274 gasification of SRF1, with a selectivity ranging between 31 and 43%, followed by CH₄ and C₂H₄. For
 275 SRF1, the selectivity in H₂, C₃H₆, C₂H₆ and C₃H₄ decreased with rising ER, while that of CH₄, C₂H₂,
 276 C₂H₄ and C₆H₆ displayed the reverse trend. For SRF2, the distribution of H-gaseous products was
 277 significantly different. Indeed, the main H-products were CH₄>C₂H₄>H₂. As SRF are very complex
 278 materials composed of a mixture of heterogeneous wastes, it is difficult to precisely discriminate the
 279 specific contribution of each component, or the interactions between each of them. However, based on
 280 the characterization performed and on the previous articles, these results tend to indicate that high
 281 plastic content in the SRF is likely responsible for the formation of stable light hydrocarbon species,

282 while the H₂ content in the syngas is low compared to syngas from biomass-rich SRF [16,31,37]. The
 283 significant content of CH₄ and C₂H₄ in syngas from SRF2 results from the decomposition of the plastic
 284 polymer chains generating various types of hydrocarbon species. Contrary to the trend observed with
 285 SRF1, the selectivity in H₂ did not decrease with rising ER for SRF2.

286 Similarly, the distribution of C atoms in the gaseous products was calculated (Figure 8). For SRF1, the
 287 two most important C-gases were CO₂ (43-54 %) and CO (22-26 %), followed by C₂H₄ (8-10 %). The
 288 selectivities in CH₄ and C₆H₆ were comparable (6-8 %) while that of other hydrocarbon species was
 289 lower than 3.6 %. The carbon distribution in syngas from SRF2 was slightly different. Although CO₂
 290 and CO were also the main products, their selectivities were significantly lower (35-50 %, and 16-19
 291 %, respectively). On the contrary, the selectivity in C₂H₄, CH₄, C₆H₆, and C₂H₂ was substantially higher
 292 than that obtained with SRF1. These results confirm that SRFs having high plastic content generate
 293 syngas rich in hydrocarbon compared to syngas from biomass-rich SRF. Moreover, these results
 294 revealed that syngas oxidation reactions were promoted by rising ER, since the distribution of carbon
 295 atoms in syngas in the form of CO₂ increased from 43 to 54% for SRF1, and from 35 to 50% for SRF2.



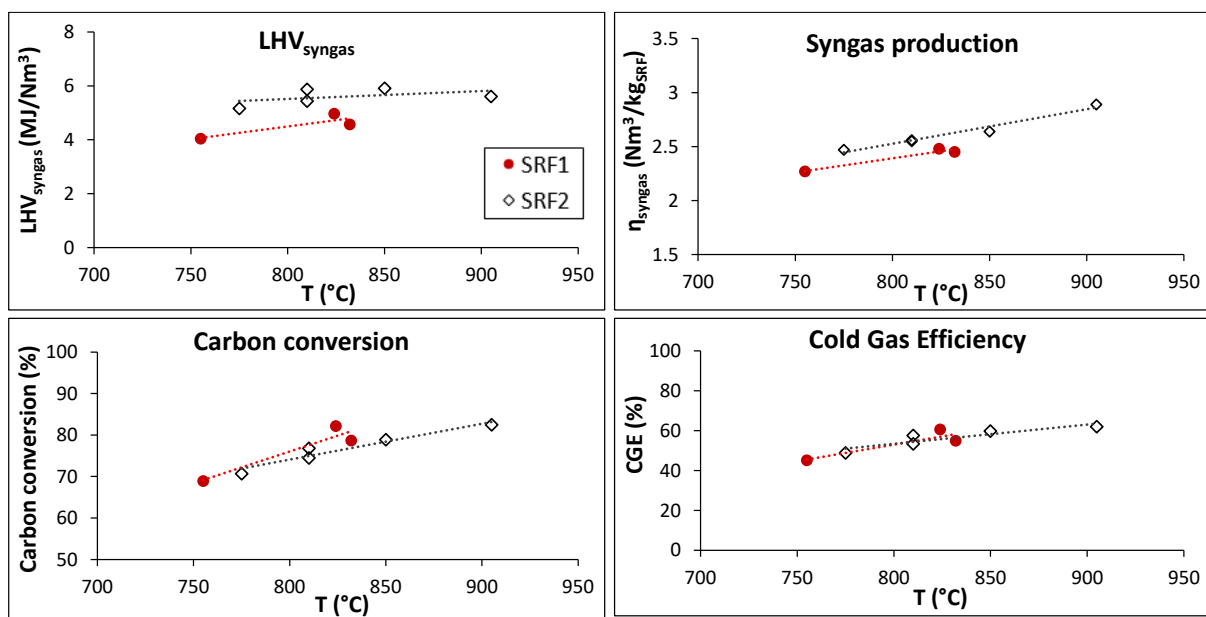
296

297 *Figure 8: Molar distribution of carbon in C-containing gases depending on the ER at a temperature*
 298 *of 800-820 °C.*

299 3.2.2 Influence of the Temperature

300 The separate influence of the temperature on the gasification efficiency was investigated by
 301 gasifying the SRFs at constant ER (0.25) while varying the reactor temperature between 750 and 905°C.

302 The evolution of the cold gas efficiency (CGE), the carbon conversion (CC), the syngas yield
 303 (η_{syngas}) and the lower heating value of the syngas ($\text{LHV}_{\text{syngas}}$) versus gasification temperature is
 304 presented in Figure 9. For the two SRFs, increasing temperature resulted in the enhancement of the
 305 gasification efficiency, as reflected by the increase in $\text{LHV}_{\text{syngas}}$, syngas production, CGE and CC.
 306 However, a problem of ash melting was encountered during the gasification of SRF1 at 880 °C, leading
 307 to the defluidization and the agglomeration of the bed. The agglomerate formed is presented in Figure
 308 10. The results of this test are not presented, as the experiment had to be stopped before to reach the
 309 steady state. This agglomeration phenomenon was not observed during the high temperature tests with
 310 the SRF2. The high content of Si and P in the SRF1 ashes (40.51 and 2.24 wt.%, respectively) could
 311 contribute to this behavior, as these species are known to melt under gasification conditions [34,38,39].



312

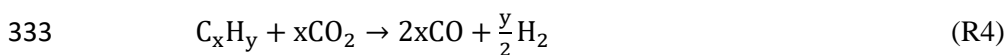
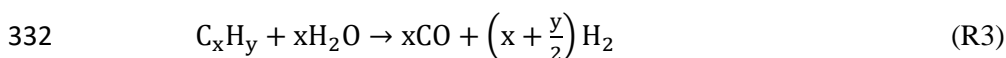
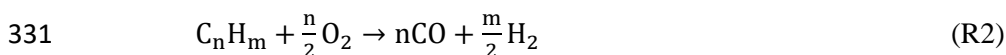
313 Figure 9: Evolution of Cold Gas Efficiency (CGE), carbon conversion (CC), syngas yield, and syngas
 314 lower heating value versus gasification temperature.

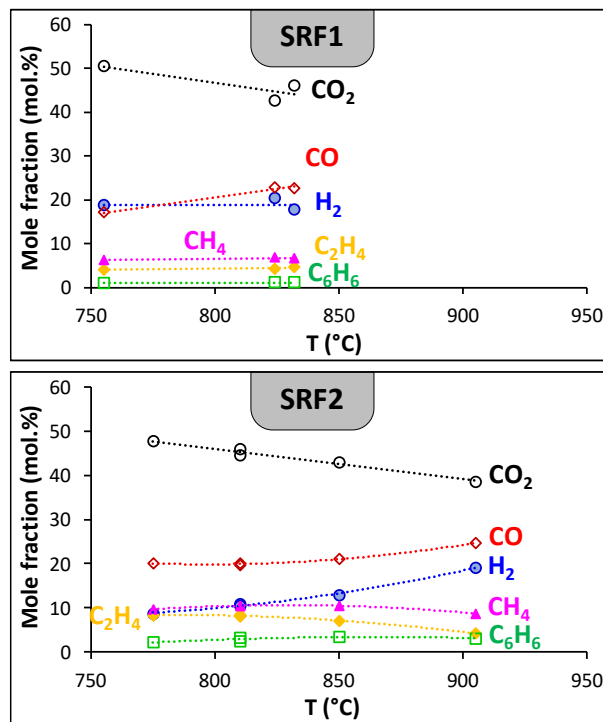


315

316 *Figure 10: Picture of the agglomerate formed in the olivine bed during the gasification of SRF1 at*
 317 *880°C.*

318 To go further in the understanding of the relationships between the SRF composition and the
 319 gasification phenomenon, the syngas composition was also studied. [Table S.2](#) (in Supplementary
 320 Material) presents syngas composition at the gasifier outlet, while [Figure 11](#) displays the composition
 321 of the gas produced by gasification reactions (nitrogen free). Whatever the nature of the SRF, the CO
 322 and H₂ contents increased with rising temperature ([Figure 11](#)). On the contrary, the CO₂ content
 323 decreased at higher temperatures. These trends can be attributed to several phenomena. Indeed, high
 324 gasification temperature can promote: the kinetic of gasification reactions generating H₂ and CO at the
 325 expense of CO₂ (R2); steam and dry reforming reactions of tar and light hydrocarbons which consume
 326 H₂O and CO₂ to produce H₂ and CO (R3 and R4); and tar cracking reactions, mainly generating H₂ and
 327 CO [21,26,27]. In addition to dry reforming reaction, the decrease in CO₂ can also be attributed to
 328 Boudouard reaction (R5), and to the Reverse Water-Gas Shift Reaction (R6). All these reactions are
 329 expected to occur simultaneously, thus explaining the syngas composition as well as the increase in
 330 gasification efficiency with rising temperature.





336

337 *Figure 11: Evolution of the composition of the gas produced (without nitrogen) versus gasification*
 338 *temperature for the different SRFs.*

339 The influence of the temperature on the distribution of hydrogen atoms in the gaseous products is
 340 presented in [Figure 12](#). For the two SRFs, rising temperature increased the selectivity in H₂, especially
 341 at temperature higher than 850 °C. This increase in H₂ was also observed for the SRF2 rich in plastics.
 342 Simultaneously, the selectivity in light hydrocarbons (C₂H₄, C₂H₆, C₃H₄, and C₃H₆) significantly
 343 decreased. These evolutions together with the drop of CO₂ strengthen the hypothesis of dry reforming
 344 reactions. The reduction of light hydrocarbon species counterbalances the increase of H₂ and CO: as a
 345 result, the LHV_{syngas} is relatively stable ([Figure 9](#)). In addition, tar reforming reactions are known to be
 346 promoted by high temperature [26,27] which can also explain the increase in H₂ and benzene (which is
 347 a product of light aromatics reforming) [40].

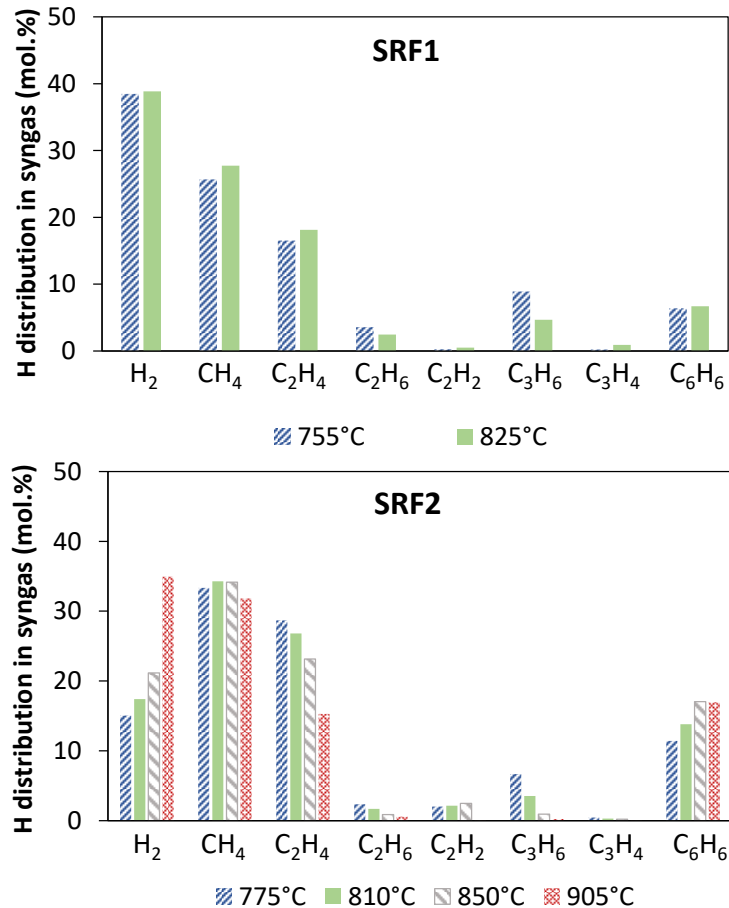


Figure 12: Distribution of hydrogen in H-containing gases depending on the gasification temperature.

4. Conclusion

This article studied the influence of the Solid Recovered Fuels (SRFs) composition and of the operating conditions on the gasification efficiency. Two industrial SRFs having different compositions were investigated. The gasification tests were performed at lab-scale in a bubbling fluidized bed using olivine as bed material, and air as gasifying agent. At industrial scale, the gasifiers are autothermal, but it is not the case at lab-scale because the wall of the small reactors must be heated to balance the heat loss. To better understand the gasification phenomena, the separate contribution of temperature and equivalence ratio (ER) on the gasification efficiency was investigated by sequentially varying these two parameters. Gasification efficiency was analyzed based on the syngas quality and on four indicators: cold gas efficiency (CGE), carbon conversion (CC), syngas lower heating value (LHV_{syngas}), and the syngas yield (η_{syngas}).

The SRFs characterization highlighted significant differences in terms of elemental and global composition. SRF1 was ash-rich (≈ 37 wt.%) while its carbon content was relatively low (≈ 35 wt.%). On the contrary, SRF2 was carbon-rich (53 wt.%) and presented low ash content (18.5 wt.%). The

365 global composition showed that SRF1 was composed of a high biomass fraction (55.2 wt.%) mainly
366 consisting in paper/carton. On the contrary, SRF2 was mainly composed of plastics (65 wt.%).

367 Gasification tests revealed that the LHV_{syngas} and the CGE significantly decreased with rising
368 equivalence ratio (ER). This evolution resulted from the oxidation reactions promoted by high ER
369 which decreased the concentration of carbonaceous gases at the expense of CO_2 , thus decreasing the
370 LHV_{syngas} . The syngas yield was proved to be almost constant with increasing ER. For these reasons,
371 the CGE decreased with rising ER. The significant amount of inorganic species (such as Ca, Na, K or
372 Fe) present in SRF1 was expected to catalyze the gasification reactions of the carbonaceous matter, thus
373 explaining the higher carbon conversion of SRF1 over SRF2. In addition, synergistic effects between
374 plastics and biomass in SRF2 could promote secondary reactions leading to char formation. The H
375 atoms distribution in syngas demonstrated that high plastic content in the SRF2 was responsible for the
376 formation of stable light hydrocarbon species, while the H_2 content in the syngas is low compared to
377 syngas from biomass-rich SRF1.

378 Increasing gasification temperature at constant ER strongly improved the gasification efficiency
379 whatever the SRF composition. Indeed, CGE, carbon conversion, syngas production and LHV_{syngas} were
380 significantly increased between 750 and 900°C. The main limitation to the use of high temperature was
381 the melting of mineral species leading to bed agglomeration and defluidization. However, this behavior
382 was only observed with SRF1 which contained large amount of Si and P, both known for their melting
383 tendency under gasification conditions. Rising temperature resulted in the increase of H_2 and CO
384 concentration in the syngas, while the concentration of CO_2 and light hydrocarbons decreased. This
385 evolution can be attributed to the several simultaneous reactions: gasification, steam and dry reforming,
386 tar cracking, Boudouard, and Reverse Water-Gas Shift. This study provides original data on the
387 influence of SRFs composition and operating conditions on the gasification efficiency and syngas
388 composition.

389 **Acknowledgements**

390 The authors acknowledge the financial support of ADEME to the Terracotta project (1606C0013).
391 The authors also thank the EDF Company, especially Emmanuel Thunin and Mathieu Insa for their
392 support on material characterizations.

393 **References**

- 394 [1] Solid Waste Management, World Bank. (n.d.).
395 <http://www.worldbank.org/en/topic/urbandevelopment/brief/solid-waste-management> (accessed
396 March 6, 2018).
397 [2] Statistiques sur les déchets - Statistics Explained, (n.d.). [http://ec.europa.eu/eurostat/statistics-
398 explained/index.php/Waste_statistics/fr](http://ec.europa.eu/eurostat/statistics-explained/index.php/Waste_statistics/fr) (accessed August 21, 2018).

- 399 [3] P.H. Brunner, L. Morf, H. Rechberger, VI.3 - Thermal waste treatment – a necessary element
400 for sustainable waste management, in: I. Twardowska (Ed.), *Waste Manag. Ser.*, Elsevier, 2004:
401 pp. 783–806. doi:10.1016/S0713-2743(04)80033-3.
- 402 [4] A. Porteous, Why energy from waste incineration is an essential component of environmentally
403 responsible waste management, *Waste Manag.* 25 (2005) 451–459.
404 doi:10.1016/j.wasman.2005.02.008.
- 405 [5] U. Arena, Process and technological aspects of municipal solid waste gasification. A review,
406 *Waste Manag.* 32 (2012) 625–639. doi:10.1016/j.wasman.2011.09.025.
- 407 [6] T.A. Milne, R. Evans, N. Abatzoglou, *Biomass Gasifier Tars: Their Nature, Formation and
408 Conversion.*, National Renewable Energy Laboratory, 1998.
- 409 [7] A. Ramos, E. Monteiro, V. Silva, A. Rouboa, Co-gasification and recent developments on
410 waste-to-energy conversion: A review, *Renew. Sustain. Energy Rev.* 81 (2018) 380–398.
411 doi:10.1016/j.rser.2017.07.025.
- 412 [8] S.K. Sansaniwal, K. Pal, M.A. Rosen, S.K. Tyagi, Recent advances in the development of
413 biomass gasification technology: A comprehensive review, *Renew. Sustain. Energy Rev.* 72
414 (2017) 363–384. doi:10.1016/j.rser.2017.01.038.
- 415 [9] N. Couto, V.B. Silva, C. Bispo, A. Rouboa, From laboratorial to pilot fluidized bed reactors:
416 Analysis of the scale-up phenomenon, *Energy Convers. Manag.* 119 (2016) 177–186.
417 doi:10.1016/j.enconman.2016.03.085.
- 418 [10] M. Campoy, A. Gómez-Barea, P. Ollero, S. Nilsson, Gasification of wastes in a pilot fluidized
419 bed gasifier, *Fuel Process. Technol.* 121 (2014) 63–69. doi:10.1016/j.fuproc.2013.12.019.
- 420 [11] U. Lee, J. Dong, J.N. Chung, Experimental investigation of sewage sludge solid waste
421 conversion to syngas using high temperature steam gasification, *Energy Convers. Manag.* 158
422 (2018) 430–436. doi:10.1016/j.enconman.2017.12.081.
- 423 [12] H. Karatas, H. Olgun, B. Engin, F. Akgun, Experimental results of gasification of waste tire
424 with air in a bubbling fluidized bed gasifier, *Fuel.* 105 (2013) 566–571.
425 doi:10.1016/j.fuel.2012.08.038.
- 426 [13] G. Xiao, M.-J. Ni, Y. Chi, K.-F. Cen, Low-temperature gasification of waste tire in a fluidized
427 bed, *Energy Convers. Manag.* 49 (2008) 2078–2082. doi:10.1016/j.enconman.2008.02.016.
- 428 [14] F. Di Gregorio, D. Santoro, U. Arena, The effect of ash composition on gasification of poultry
429 wastes in a fluidized bed reactor, *Waste Manag. Res.* 32 (2014) 323–330.
430 doi:10.1177/0734242X14525821.
- 431 [15] M.L. Mastellone, L. Zaccariello, U. Arena, Co-gasification of coal, plastic waste and wood in a
432 bubbling fluidized bed reactor, *Fuel.* 89 (2010) 2991–3000. doi:10.1016/j.fuel.2010.05.019.
- 433 [16] U. Arena, F. Di Gregorio, Energy generation by air gasification of two industrial plastic wastes
434 in a pilot scale fluidized bed reactor, *Energy.* 68 (2014) 735–743.
435 doi:10.1016/j.energy.2014.01.084.
- 436 [17] N.D. Couto, V.B. Silva, A. Rouboa, Assessment on steam gasification of municipal solid waste
437 against biomass substrates, *Energy Convers. Manag.* 124 (2016) 92–103.
438 doi:10.1016/j.enconman.2016.06.077.
- 439 [18] B. Hu, Q. Huang, A. Buekens, Y. Chi, J. Yan, Co-gasification of municipal solid waste with
440 high alkali coal char in a three-stage gasifier, *Energy Convers. Manag.* 153 (2017) 473–481.
441 doi:10.1016/j.enconman.2017.10.026.
- 442 [19] M.P. González-Vázquez, R. García, M.V. Gil, C. Pevida, F. Rubiera, Comparison of the
443 gasification performance of multiple biomass types in a bubbling fluidized bed, *Energy
444 Convers. Manag.* 176 (2018) 309–323. doi:10.1016/j.enconman.2018.09.020.

- 445 [20] V. Silva, A. Rouboa, Combining a 2-D multiphase CFD model with a Response Surface
446 Methodology to optimize the gasification of Portuguese biomasses, *Energy Convers. Manag.* 99
447 (2015) 28–40. doi:10.1016/j.enconman.2015.03.020.
- 448 [21] G. Dunnu, K.D. Panopoulos, S. Karellas, J. Maier, S. Toulou, G. Koufodimos, I. Boukis, E.
449 Kakaras, The solid recovered fuel Stabilat®: Characteristics and fluidised bed gasification tests,
450 *Fuel*. 93 (2012) 273–283. doi:10.1016/j.fuel.2011.08.061.
- 451 [22] F. Pinto, R.N. André, C. Carolino, M. Miranda, P. Abelha, D. Direito, N. Perdikaris, I. Boukis,
452 Gasification improvement of a poor quality solid recovered fuel (SRF). Effect of using natural
453 minerals and biomass wastes blends, *Fuel*. 117 (2014) 1034–1044.
454 doi:10.1016/j.fuel.2013.10.015.
- 455 [23] J. Corella, J.M. Toledo, R. Padilla, Olivine or Dolomite as In-Bed Additive in Biomass
456 Gasification with Air in a Fluidized Bed: Which Is Better?, *Energy Fuels*. 18 (2004) 713–720.
457 doi:10.1021/ef0340918.
- 458 [24] L. Devi, K.J. Ptasinski, F.J.J.G. Janssen, S.V.B. van Paasen, P.C.A. Bergman, J.H.A. Kiel,
459 Catalytic decomposition of biomass tars: use of dolomite and untreated olivine, *Renew. Energy*.
460 30 (2005) 565–587. doi:10.1016/j.renene.2004.07.014.
- 461 [25] Y. Shen, J. Wang, X. Ge, M. Chen, By-products recycling for syngas cleanup in biomass
462 pyrolysis – An overview, *Renew. Sustain. Energy Rev.* 59 (2016) 1246–1268.
463 doi:10.1016/j.rser.2016.01.077.
- 464 [26] J. Recari, C. Berruoco, S. Abelló, D. Montané, X. Farriol, Gasification of two solid recovered
465 fuels (SRFs) in a lab-scale fluidized bed reactor: Influence of experimental conditions on
466 process performance and release of HCl, H₂S, HCN and NH₃, *Fuel Process. Technol.* 142
467 (2016) 107–114. doi:10.1016/j.fuproc.2015.10.006.
- 468 [27] C. Berruoco, J. Recari, S. Abelló, X. Farriol, D. Montané, Experimental Investigation of Solid
469 Recovered Fuel (SRF) Gasification: Effect of Temperature and Equivalence Ratio on Process
470 Performance and Release of Minor Contaminants, *Energy Fuels*. 29 (2015) 7419–7427.
471 doi:10.1021/acs.energyfuels.5b02032.
- 472 [28] U. Arena, F. Di Gregorio, Fluidized bed gasification of industrial solid recovered fuels, *Waste*
473 *Manag.* 50 (2016) 86–92. doi:10.1016/j.wasman.2016.02.011.
- 474 [29] L. Devi, K.J. Ptasinski, F.J.J.G. Janssen, A review of the primary measures for tar elimination in
475 biomass gasification processes, *Biomass Bioenergy*. 24 (2003) 125–140. doi:10.1016/S0961-
476 9534(02)00102-2.
- 477 [30] U. Arena, L. Zaccariello, M.L. Mastellone, Fluidized bed gasification of waste-derived fuels,
478 *Waste Manag.* 30 (2010) 1212–1219. doi:10.1016/j.wasman.2010.01.038.
- 479 [31] A. Gómez-Barea, P. Ollero, B. Leckner, Optimization of char and tar conversion in fluidized
480 bed biomass gasifiers, *Fuel*. 103 (2013) 42–52. doi:10.1016/j.fuel.2011.04.042.
- 481 [32] G. Lardier, J. Kaknics, A. Dufour, R. Michel, B. Cluet, O. Authier, J. Poirier, G. Mauviel, Gas
482 and Bed Axial Composition in a Bubbling Fluidized Bed Gasifier: Results with Miscanthus and
483 Olivine, *Energy Fuels*. 30 (2016) 8316–8326. doi:10.1021/acs.energyfuels.6b01816.
- 484 [33] GE Jenbacher, Fuel gas quality, special gases, 2009.
- 485 [34] C. Dupont, S. Jacob, K.O. Marrakchy, C. Hognon, M. Grateau, F. Labalette, D. Da Silva Perez,
486 How inorganic elements of biomass influence char steam gasification kinetics, *Energy*. 109
487 (2016) 430–435. doi:10.1016/j.energy.2016.04.094.
- 488 [35] K.G. Burra, A.K. Gupta, Synergistic effects in steam gasification of combined biomass and
489 plastic waste mixtures, *Appl. Energy*. 211 (2018) 230–236. doi:10.1016/j.apenergy.2017.10.130.
- 490 [36] A. Ephraim, D. Pham Minh, D. Lebonnois, C. Peregrina, P. Sharrock, A. Nzihou, Co-pyrolysis
491 of wood and plastics: Influence of plastic type and content on product yield, gas composition
492 and quality, *Fuel*. 231 (2018) 110–117. doi:10.1016/j.fuel.2018.04.140.

- 493 [37] U. Arena, F. Di Gregorio, Gasification of a solid recovered fuel in a pilot scale fluidized bed
494 reactor, *Fuel*. 117 (2014) 528–536. doi:10.1016/j.fuel.2013.09.044.
- 495 [38] C. Hognon, C. Dupont, M. Grateau, F. Delrue, Comparison of steam gasification reactivity of
496 algal and lignocellulosic biomass: Influence of inorganic elements, *Bioresour. Technol.* 164
497 (2014) 347–353. doi:10.1016/j.biortech.2014.04.111.
- 498 [39] A. Nzihou, B. Stanmore, The fate of heavy metals during combustion and gasification of
499 contaminated biomass—A brief review, *J. Hazard. Mater.* 256–257 (2013) 56–66.
500 doi:10.1016/j.jhazmat.2013.02.050.
- 501 [40] A. Dufour, P. Girods, E. Masson, Y. Rogaume, A. Zoulalian, Synthesis gas production by
502 biomass pyrolysis: Effect of reactor temperature on product distribution, *Int. J. Hydrog. Energy*.
503 34 (2009) 1726–1734. doi:10.1016/j.ijhydene.2008.11.075.
- 504

505 **Supplementary information**

506 *Table S.1: Syngas composition (in mol.%) at the gasifier outlet depending on the SRF for different*
 507 *Equivalent Ratio at a temperature of 800-820°C.*

SRF	SRF1				SRF2			
	ER	0.21	0.25	0.30	0.35	0.21	0.25	0.30
H ₂	9.92	6.70	4.25	3.20	4.00	3.31	3.43	2.46
O ₂	0.00	0.08	0.53	0.00	0.14	0.04	0.14	0.11
CO	9.42	8.00	6.46	6.12	7.27	6.18	5.53	4.57
CO ₂	15.85	15.60	15.13	14.98	14.46	14.08	14.57	13.87
C ₂ H ₄	1.76	1.55	1.34	1.13	3.31	2.55	2.06	1.44
C ₂ H ₆	0.21	0.14	0.09	0.05	0.16	0.11	0.07	0.04
C ₂ H ₂	0.06	0.09	0.13	0.16	0.41	0.41	0.37	0.33
CH ₄	2.94	2.38	1.89	1.66	4.15	3.26	2.63	2.07
C ₃ H ₆	0.43	0.27	0.15	0.08	0.34	0.22	0.13	0.04
C ₃ H ₄	0.11	0.08	0.02	0.02	0.04	0.03	0.01	0.01
C ₆ H ₆	0.44	0.38	0.35	0.34	1.05	0.88	0.22	0.55
N ₂	53.39	58.64	64.63	65.86	63.70	67.19	69.62	73.60

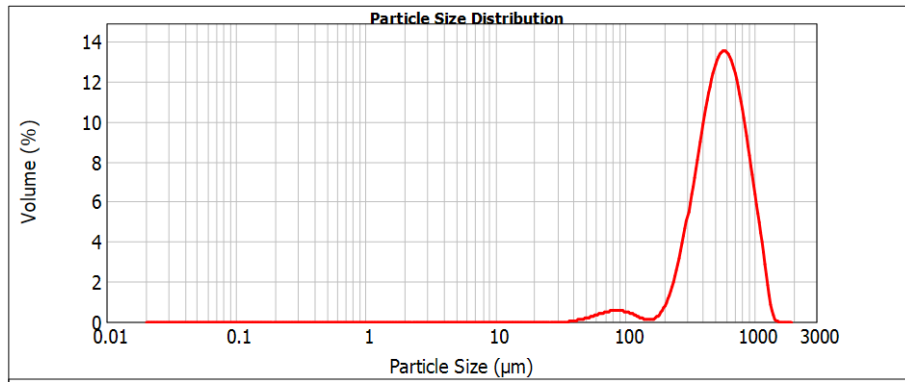
508

509

510

511 *Table S.2: Syngas composition at the gasifier outlet depending on the SRF for different temperatures.*

SRF	SRF1			SRF2			
	T (°C)	755	825	880	775	810	850
H ₂	6.08	6.70	9.55	2.63	3.31	4.09	6.61
O ₂	0.13	0.08	0.00	0.08	0.04	0.01	0.49
CO	5.56	8.00	15.63	6.05	6.18	6.67	8.54
CO ₂	16.48	15.60	11.96	14.37	14.08	13.63	13.38
C ₂ H ₄	1.31	1.55	1.75	2.50	2.55	2.264	1.45
C ₂ H ₆	0.19	0.14	0.11	0.14	0.11	0.06	0.04
C ₂ H ₂	0.04	0.09	0.15	0.35	0.41	0.48	0.02
CH ₄	2.03	2.38	3.00	2.90	3.26	3.30	3.01
C ₃ H ₆	0.47	0.27	0.12	0.39	0.22	0.06	0.02
C ₃ H ₄	0.02	0.08	0.00	0.04	0.03	0.02	0.01
C ₆ H ₆	0.34	0.38	0.50	0.66	0.88	1.10	1.07
N ₂	63.70	58.64	50.24	69.63	67.19	64.99	59.46



512

513

Figure S.1: Particle size distribution of fresh olivine.